Metallacycle-cored supramolecular assemblies with tunable fluorescence including white-light emission

Mingming Zhang[a], Shouchun Yin[a,b,1], Jing Zhang[b], Zhixuan Zhou[a], Manik Lal Saha[a], Chenjie Lu[b], and Peter J. Stang[a,1]

[a]Department of Chemistry, University of Utah, Salt Lake City, UT 84112; and [b]College of Material, Chemistry and Chemical Engineering, Hangzhou Normal University, Hangzhou 310036, People's Republic of China

Contributed by Peter J. Stang, February 14, 2017 (sent for review December 20, 2016; reviewed by Gabor A. Somorjai and Vivian Wing-Wah Yam)

Control over the fluorescence of supramolecular assemblies is crucial for the development of chemosensors and light-emitting materials. Consequently, the postsynthetic modification of supramolecular structures via host–guest interactions has emerged as an efficient strategy in recent years that allows the facile tuning of the photophysical properties without requiring a tedious chemical synthesis. Herein, we used a phenanthrene-21-crown-7 (P21C7)-based 60° diplatinum(II) acceptor 8 in the construction of three exohedral P21C7 functionalized rhomboidal metallacycles 1–3 which display orange, cyan, and green emission colors, respectively. Although these colors originate from the dipyridyl precursors 10–12, containing triphenylamine-, tetraphenylethene-, and pyrene-based fluorophores, respectively, the metal–ligand coordination strongly influences their emission properties. The metallacycles were further linked into emissive supramolecular oligomers by the addition of a fluorescent bis-ammonium linker 4 that forms complementary host–guest interactions with the pendant P21C7 units. Notably, the final ensemble derived from a 1:1 mixture of 1 and 4 displays a concentration-dependent emission. At low concentration, i.e., <25 μM, it emits a blue color, whereas an orange emission was observed when the concentration exceeds >5 mM. Moreover, white-light emission was observed from the same sample at a concentration of 29 μM, representing a pathway to construct supramolecular assemblies with tunable fluorescence properties.

fluorescence | supramolecular metallacycles | host–guest interactions | white-light emission | orthogonal interactions

Fluorescent supramolecular assemblies have received much attention due to their broad applications as biological and chemical sensors (1–5), bioimaging agents (6–10), light-emitting materials (11–15), etc. One method used to prepare such assemblies is coordination-driven self-assembly (16–29), because the incorporation of metal coordination not only endows the resultant assemblies with good stabilities but also at times provides unique emissions that are different from the fluorescent ligands and/or metal ions. By the incorporation of tetraphenylene derivatives into supramolecular coordination complexes (SCC) platforms, our group has prepared a series of highly emissive metal–organic assemblies that are capable of sensing nitroaromatics, cell imaging, etc. (30–34), although the precursors are weakly- or nonemissive. Similarly, Yoshizawa and coworkers prepared a series of M_2L_4 (M = Zn, Cu, Pt, Ni, Co, and Mn) capsules among which only the Zn(II) capsule emits blue fluorescence with a quantum yield of 80%, whereas the other capsules are nonemissive (35).

Fluorophores with aggregation-induced emission (AIE) (36–39) properties are good candidates for the construction of fluorescent supramolecular polymers because both the formation of supramolecular polymers and the accomplishment of a reasonable emission from the AIE cores need high concentrations. However, supramolecular oligomers/polymers with tunable emission have been rarely reported, although some progress has recently been made on the construction of discrete fluorescent supramolecular assemblies (29). The introduction of additional fluorophores via noncovalent interactions provides an alternative approach to further tune the emission of a given SCC (40, 41), leading to the formation of fluorescent supramolecular polymers. Herein we report three emissive metallacycles with pendant crown ether units by the incorporation of three different fluorescent dipyridyl ligands. Upon the addition of a fluorescent bis-ammonium linker, supramolecular oligomers are formed and the emission properties of these metallacycles were further tuned. Moreover, using the orange-emissive metallacycle **1** with AIE properties and the blue-emissive linker **4** with aggregation-caused quenching (ACQ) properties (39), the emission of the resultant supramolecular oligomers can be tuned from orange to blue as the concentration decreases. Interestingly, the same sample emits white-light emission at a concentration of 29 μM. This is an example where white-light emission was achieved by the integration of complementary emission properties (AIE and ACQ), complementary colors (orange and blue), and complementary host–guest interactions (crown ether and ammonium salts).

Results and Discussion

The synthetic procedures for rhomboidal metallacycles **1**, **2**, and **3** and a bis-ammonium linker **4** are shown in Fig. 1. A phenanthrene-21-crown-7 (P21C7)-based 60° diplatinum(II) acceptor **8** was synthesized in a three-step pathway starting from 3,6-dibromophenanthrene-9,10-diol **5** (Fig. 1*A*). The key intermediate 3,6-dibromophenanthrene-21-crown-7 **6** was prepared by a potassium-templated cyclization reaction of **5** and hexethylene glycol ditosylate. The oxidative addition of **6** to $Pt(PEt_3)_4$ at each bromide site furnished **7**, whose bromide anions were then exchanged by treating with AgOTf, leading to the formation of **8** in a good yield. The rhomboidal Pt(II) metallacycles **1**, **2**, and **3** were prepared by stirring the 60° platinum acceptor **8** and the corresponding 120°

Significance

Light-emitting materials have been widely studied for their promising applications in chemical and biological science. Here we report three phenanthrene-21-crown-7 functionalized fluorescent Pt(II) rhomboidal metallacycles which were then converted into fluorescent supramolecular oligomers by reacting with a bis-ammonium linker. One of these constructs shows concentration-dependent fluorescence in a wide color range, where orange emission at high concentration and blue emission at low concentration was observed. Moreover, at a concentration of 29 μM the same ensemble emits white light that has emerged from the integration of the complementary orange and blue color from the metallacycles and linker, respectively. This study shows how light-emitting materials can be obtained by the proper implementation of multiple orthogonal interactions in a single process.

Author contributions: M.Z., S.Y., and P.J.S. designed research; M.Z., S.Y., J.Z., Z.Z., M.L.S., and C.L. performed research; M.Z. and S.Y. contributed new reagents/analytic tools; M.Z. and S.Y. analyzed data; and M.Z., S.Y., M.L.S., and P.J.S. wrote the paper.

Reviewers: G.A.S., University of California, Berkeley; and V.W.-W.Y., The University of Hong Kong.

The authors declare no conflict of interest.

[1]To whom correspondence may be addressed. Email: yinsc@hznu.edu.cn or stang@chem.utah.edu.

This article contains supporting information online at www.pnas.org/lookup/suppl/doi:10.1073/pnas.1702510114/-/DCSupplemental.

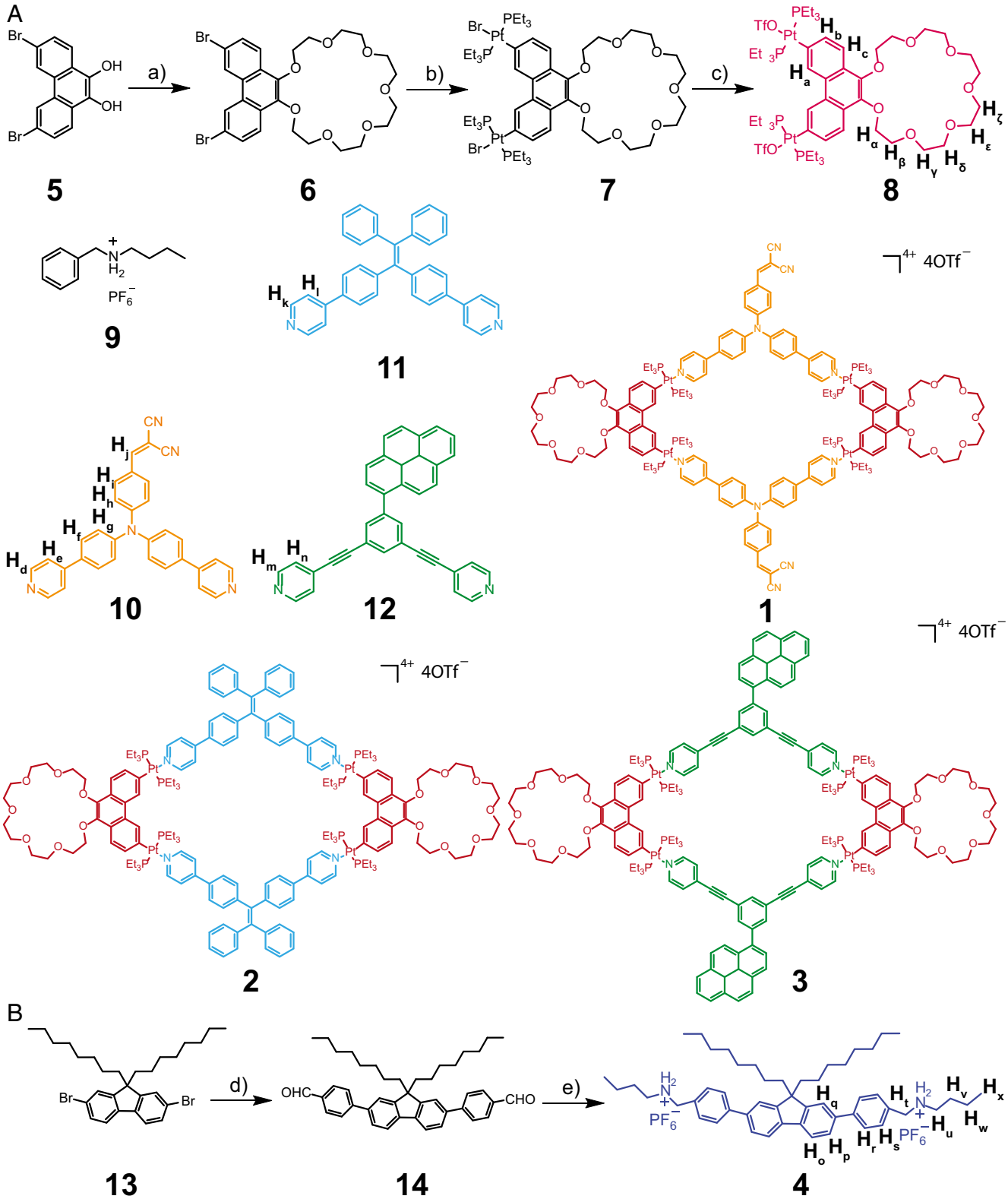

Fig. 1. Synthetic routes and chemical structures of compounds. Synthetic routes of 60° diplatinum (II) acceptor **8** (*A*) and bis-ammonium linker **4** (*B*). Conditions: a) hexethylene glycol ditosylate, K_2CO_3, CH_3CN, reflux, 72 h; 64%; b) $Pt(PEt_3)_4$, toluene, 95 °C, 72 h; 68%; c) AgOTf, dry CH_2Cl_2, room temperature, 12 h; 95%; d) (4-formylphenyl)boronic acid, K_2CO_3, $Pd(PPh_3)_4$, dioxane/water (2:1), 90 °C, 48 h; 63%; e) (*i*) *n*-butylamine, CH_3OH, reflux, 12h; (*ii*) $NaBH_4$, room temperature, 24 h; (*iii*) HCl (aq), and (*iv*) NH_4PF_6 (aq); 27% in four steps.

dipyridyl donor **10**, **11**, or **12**, respectively, in dichloromethane at room temperature for 24 h. The bis-ammonium linker **4** was prepared from commercially available 2,7-dibromo-9,9-dioctyl-9*H*-fluorene **13** (Fig. 1*B*). Reaction of **13** with (4-formylphenyl)boronic acid via a Suzuki coupling provided compound **14** with two aldehyde groups, which were further reacted to afford bis-ammonium salt **4**.

The formation of metallacycles **1**, **2**, and **3** was confirmed by multinuclear NMR (^{31}P and ^{1}H) analysis and electrospray ionization time-of-flight mass spectrometry (ESI-TOF-MS). The ^{31}P{^{1}H}

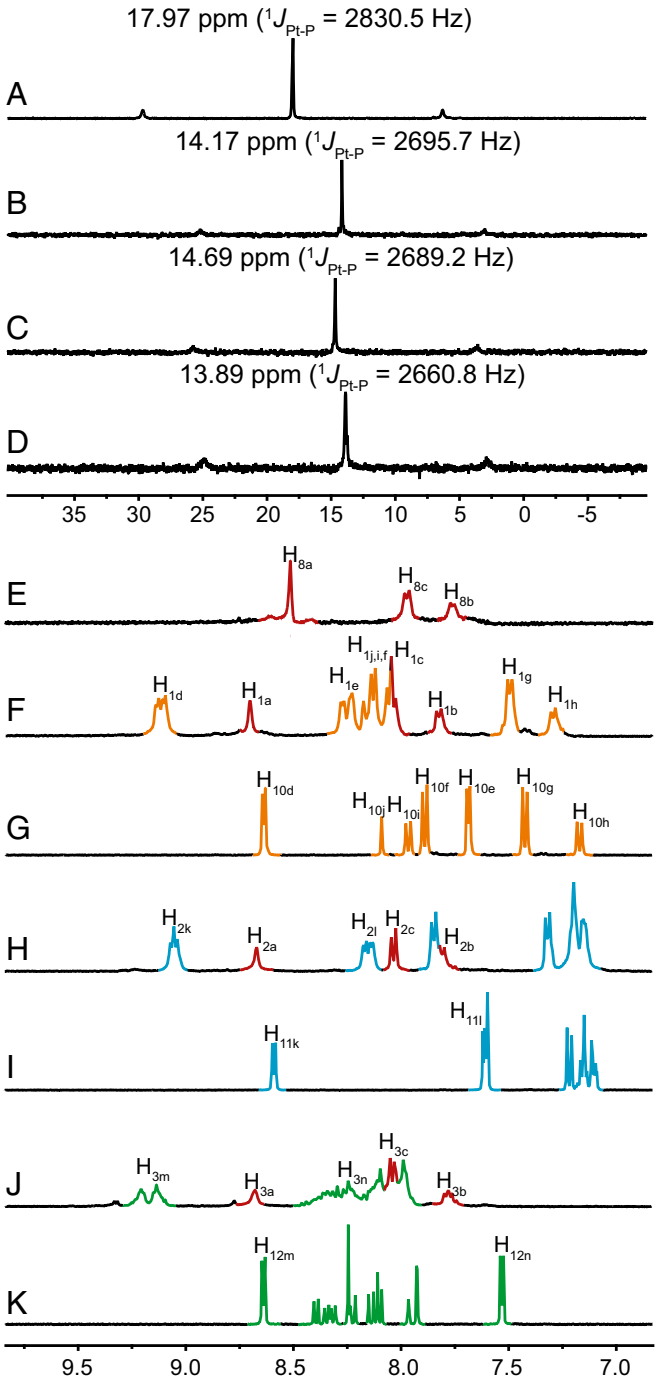

Fig. 2. NMR characterization ligands **8**, **10**, **11**, and **12** and metallacycles **1**, **2**, and **3**. Partial (*A*–*D*) ^{31}P and (*E*–*K*) ^{1}H NMR spectra (CD_3COCD_3, 295 K) of platinum acceptor **8** (*A* and *E*), ligands **10** (*G*), **11** (*I*), and **12** (*K*), and metallacycles **1** (*B* and *F*), **2** (*C* and *H*), and **3** (*D* and *J*).

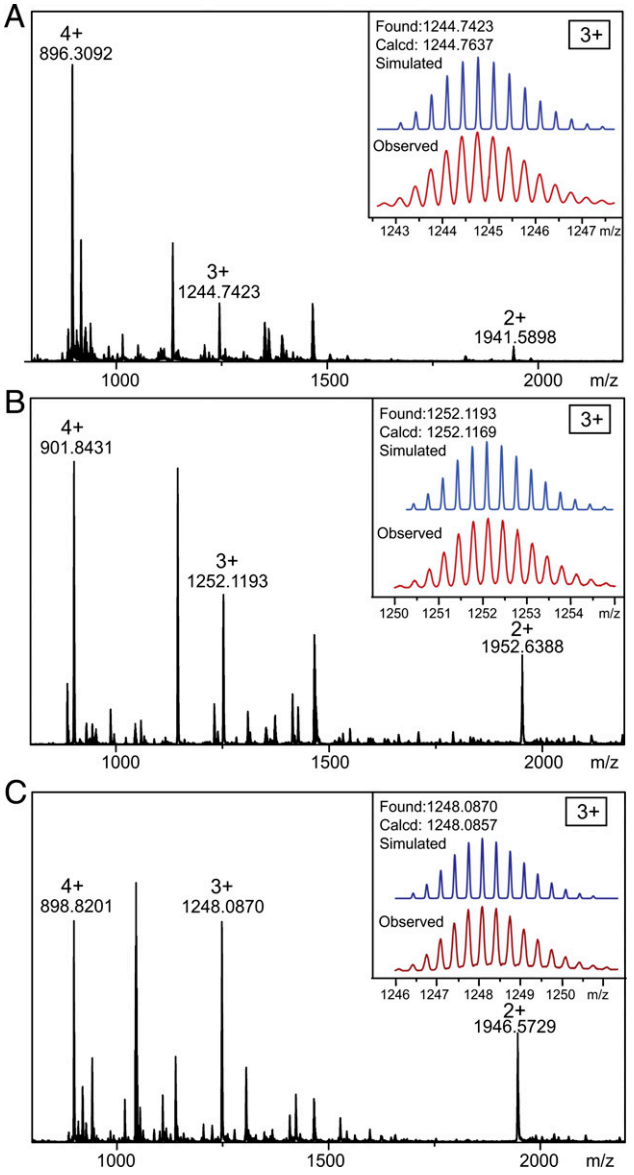

Fig. 3. Mass spectra of metallacycles **1** (*A*), **2** (*B*), and **3** (*C*).

NMR spectra of **1**, **2**, and **3** exhibit sharp singlets with concomitant ^{195}Pt satellites at 14.17 ppm for **1**, 14.69 ppm for **2**, and 13.89 ppm for **3** (Fig. 2, spectra *B*–*D*), corresponding to a single phosphorous environment, indicating the formation of discrete, highly symmetric metallacycles (31–34). In the ^{1}H NMR spectra of these metallacycles, downfield chemical shifts were observed for the α-pyridyl protons H_d (from 8.64 to 9.13 and 9.10 ppm), H_k (from 8.59 to 9.07 and 9.05 ppm), and H_m (from 8.64 to 9.22 and 9.15 ppm) and β-pyridyl protons H_e (from 7.69 to 8.24 and 8.15 ppm), H_l (from 7.61 to 8.17 and 8.15 ppm), and H_n (from 7.53 to 8.31 and 8.26 ppm) and both split into two set of signals (Fig. 2, spectra *F*–*K*). The aromatic protons of H_a, H_b, and H_c of platinum(II) acceptor also shifted downfield. All these chemical shift changes are similar to their analogous reaction systems (31–34), providing evidence for the formation of rhomboidal metallacycles. ESI-TOF-MS provided evidence for the stoichiometry of formation of discrete rhomboidal Pt(II) metallacycles. Prominent sets of peaks with charge states (from 2+ to 4+) were observed for all of the metallacycles due to the loss of counterions (OTf^-), and each peak closely matched the

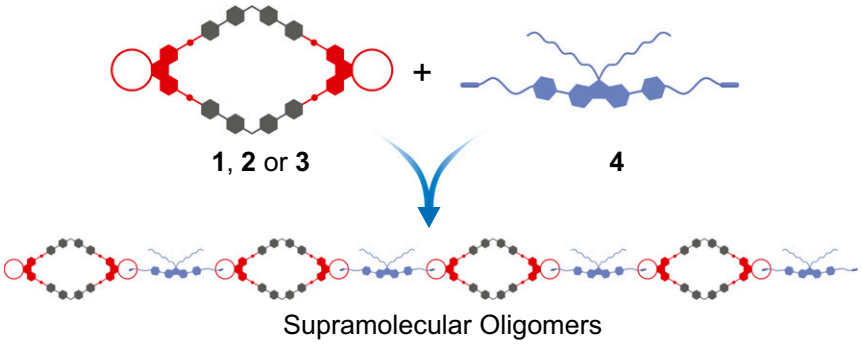

Fig. 4. Cartoon representation of the formation of supramolecular oligomers.

corresponding simulated isotope pattern (Fig. 3), supporting the composition of **1**–**3**.

The complexation between crown ether **8** and secondary ammonium salt **9** was first investigated as a model system (*SI Appendix*, Figs. S34–S36). The association constant (K_a) of **8·9** in acetone was determined by a ^{1}H NMR titration method, with a value of 9.4 ($\pm$1.0) $\times$ 10^2 M^{-1}, which is comparable to that of benzo-21-crown-7·**9** (6.2 ($\pm$0.4) $\times$ 10^2 M^{-1}) (42) and suitable for the construction of supramolecular assemblies (Fig. 4).

Concentration-dependent ^{1}H NMR measurements were then carried out to study the formation of the supramolecular oligomers. Therefore, a 1:1 mixture of **1** and **4** was chosen as the onset. The concentration of the sample was increased from 1.0 mM to 40.0 mM, leading to noticeable chemical shift changes for both precursors. Upfield chemical shifts were observed for the benzyl protons H_t and methylene protons H_u of the bis-ammonium linker **4**, whereas the ethyl protons H_α and H_β of the metallacycle **1** shifted downfield (Fig. 5). Moreover, the chemical shifts of the linker **4** in the latter ensemble appeared in a similar region to that of **9** in the complex **8·9**, indicating the formation of supramolecular oligomers via host–guest complexation. Two-dimensional diffusion-ordered NMR experiments were also carried out to test the size of the supramolecular oligomers in solution. As the concentration of the sample increased from 5.00 to 40.0 mM, the measured weight average diffusion coefficient (D) decreased from 3.19 $\times$ 10^{-10} to 1.16 $\times$ 10^{-10} $m^2{\cdot}s^{-1}$ (*SI Appendix*, Fig. S37), indicating the formation of high molecular weight supramolecular assemblies (43–46). To investigate the effect of the counterions in the assembly process, the counterions of **4** were also changed from hexafluorophosphate (PF_6) to trifluoromethanesulfonate (OTf) anions and the ^{1}H NMR spectrum of a mixture of **1** and **4•OTf** at 5 mM was measured (*SI Appendix*, Fig. S38). However, this shows negligible effects compared with the ^{1}H NMR spectrum of a mixture containing **1** and **4**•PF_6 salt, suggesting that the counterions do not influence these assembly processes.

The UV-vis absorption and emission spectra of ligands **10**, **11**, and **12**, rhomboidal metallacycles **1**, **2**, and **3** and bis-ammonium linker **4** in acetone are shown in Fig. 6. Ligand **10** displays two broad absorption bands centered at 346 and 440 nm with molar absorption coefficients (ε) of 2.28 $\times$ 10^4 $M^{-1}{\cdot}cm^{-1}$ and 4.09 $\times$ 10^4 $M^{-1}{\cdot}cm^{-1}$, respectively (Fig. 6, spectrum *A*). Ligand **11** shows one broad absorption band in the range of 320–370 nm, whereas ligand **12** exhibits one broad absorption band centered at 344 nm with ε = 3.03 $\times$ 10^4 $M^{-1}{\cdot}cm^{-1}$. Metallacycle **1** exhibits two absorption bands centered at 380 and 436 nm with ε = 9.13 $\times$ 10^4 $M^{-1}{\cdot}cm^{-1}$ and 8.04 $\times$ 10^4 $M^{-1}{\cdot}cm^{-1}$, respectively (Fig. 6, spectrum *A*). There is one absorption band centered at 322 nm for **2**, 323 nm for **3**, and 331 nm for **4** with ε = 1.16 $\times$ 10^5 $M^{-1}{\cdot}cm^{-1}$, 1.77 $\times$ 10^5 $M^{-1}{\cdot}cm^{-1}$, and 3.85 $\times$ 10^4 $M^{-1}{\cdot}cm^{-1}$, respectively. It is worth noting that the absorption of metallacycles **1**, **2**, and **3** is greatly increased compared with their precursors **10**, **11**, and **12** due to the inclusion of multiple ligands in one metallacycle structure.

Ligands **10**, **11**, and **12** display moderate emission bands centered at 465, 472, and 445 nm in acetone, respectively (Fig. 6, spectrum *B*). Upon the formation of rhomboidal metallacycles, red-shifts were observed for **1** and **2**. Specifically, rhomboids **1**, **2**, and **3** exhibit one emission band centered at 563, 490, and 445 nm, respectively, corresponding to the orange, cyan, and green emission according to the 1931 Commission Internationale de L'Eclairage (CIE) chromaticity diagram. Bis-ammonium linker **4** shows two emission bands centered at 391 and 411 nm, corresponding to the blue emission. Compared with their dipyridyl precursors **10**, **11**, and **12**, the emissions of metallacycles **1** and **3** decrease whereas that of metallacycle **2** increases. The decrease of the emission is due to heavy atom effect which was also observed in other SCC systems (29). Although this effect also influences the

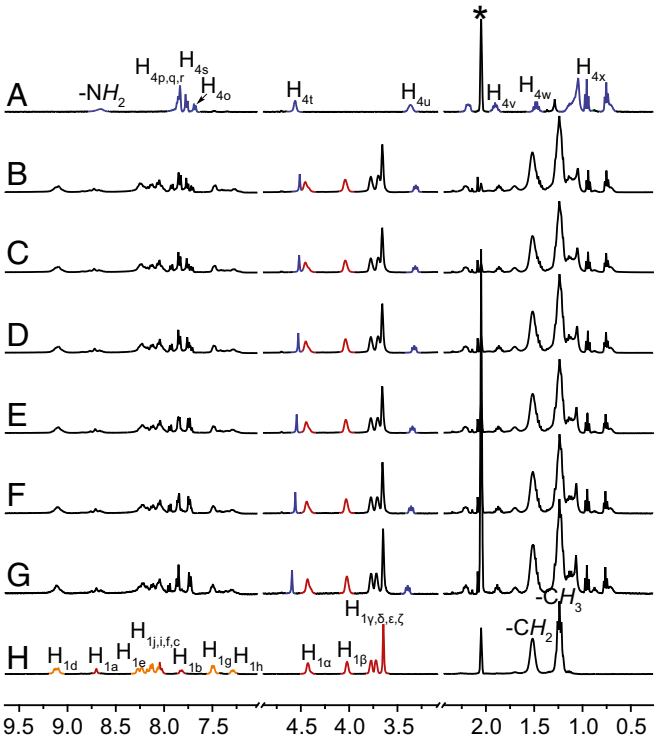

Fig. 5. Partial ^{1}H NMR spectra (CD_3COCD_3, 295 K, 400 MHz) of bis-ammonium linker **4** (*A*), and equal molar **4** and **1** at the concentration of 40 mM (*B*), 30 mM (*C*), 20 mM (*D*), 10 mM (*E*), 5.0 mM (*F*), 1.0 mM (*G*), and metallacycle **1** (*H*). The acetone peaks are marked with asterisks.

CHEMISTRY

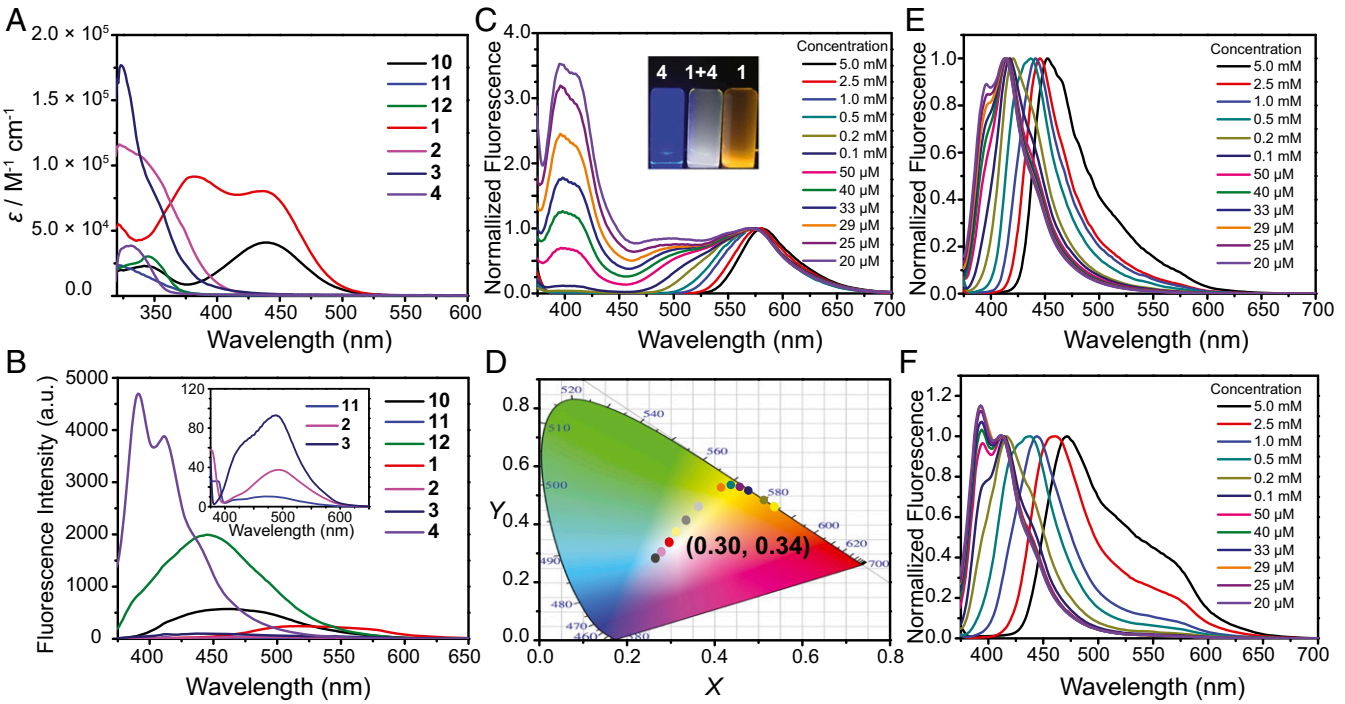

Fig. 6. Spectral characterization of ligands **10**, **11**, **12**, metallacycles **1**, **2**, **3**, and bis-ammonium linker **4**. (*A*) UV-vis absorption spectra of ligands **10**, **11**, **12**, metallacycles **1**, **2**, **3**, and bis-ammonium linker **4** in acetone (c = 10 μM). (*B*) Emission spectra of ligands **10**, **11**, **12**, metallacycles **1**, **2**, **3**, and bis-ammonium linker **4** in acetone (λ_{ex} = 365 nm, c = 10 μM). (*C*) Emission spectra of equal molar **1** and **4** at different concentrations; (*Inset*) photograph of **1**, **4**, and mixture of equal molar **1** and **4** in acetone upon excitation at 365 nm using a UV lamp at 298 K (c = 29 μM). (*D*) CIE chromaticity coordinates of equal molar **1** and **4** at different concentrations, according to the fluorescence spectra recorded in *C*. (*E*) Emission spectra of equal molar **2** and **4** at different concentrations. (*F*) Emission spectra of equal molar **3** and **4** at different concentrations.

emission of **2**, the metal coordination inhibits the free rotation of the aromatic rings of the tetraphenylene derivatives, which enhances the emission of **2** relative to **11** (31–34).

The emission properties of the supramolecular assemblies formed by metallacycles (**1**, **2**, or **3**) and bis-ammonium **4** were investigated (Fig. 6, spectrum *C*). Interestingly, the supramolecular assemblies formed by **1** and **4** (1:1 molar ratio) show concentration-dependent fluorescence in a wide color range, where an orange emission at high concentration (>0.5 mM) and a blue emission at low concentration (<25 μM) were observed. This is likely because in the ensemble the metallacycle **1** acts as an AIE fluorophore, whereas the bis-ammonium linker **4** is an ACQ fluorophore (*SI Appendix*, Figs. S39 and S40). At high concentration, the AIE fluorophore plays a more important role so the sample mainly shows orange emission derived from **1**. However, at low concentration, the ACQ fluorophore dominates the fluorescence, thus the ensemble exhibits a blue emission derived from **4**. Moreover, the same sample displays white-light emission (CIE chromaticity coordinate: 0.30, 0.34) at a concentration of 29 μM (Fig. 6, spectrum *D*), which has only been rarely found in such supramolecular assemblies. At 29 μM, both the orange emission and the blue emission are observed and the emission covers the entire visible spectral region (400~700 nm), endowing the solution with an overall white-light emission. Tunable emission was also observed in the assemblies formed by **2** and **4** or **3** and **4** (Fig. 6, spectra *E* and *F*). However, in these two assemblies, the color of the emission cannot be tuned in a wide range because of the strong overlap between the emission of **2** (or **3**) and **4**. This study provides a simple yet efficient approach for finely tuning the emission of supramolecular assemblies via concentration by the incorporation of both AIE and ACQ fluorophores as their building blocks.

Conclusion

In summary, three Pt(II) rhomboidal metallacycles with orange (**1**), cyan (**2**), and green (**3**) emissions were prepared by the metal-coordination-driven self-assembly of the 60° diplatinum(II) acceptor **8** and 120° dipyridyl donors **10**–**12**. Supramolecular oligomers were further obtained via the host–guest interactions between the P21C7 units of the metallacyles and ammonium salts. The emissions of these supramolecular assemblies as well as their precursors were studied. These supramolecular oligomers show concentration-dependent fluorescence. Notably, the assemblies formed by orange-emissive metallacycle **1** and blue-emissive bis-ammonium linker **4** emit from orange to blue as the concentration decreases, whereas white-light emission was obtained at the concentration of 29 μM. This study provides a strategy to prepare light-emitting metal–organic assemblies by the precise manipulation of the AIE and ACQ properties (39) of the fluorophores.

Materials and Methods

All reagents and deuterated solvents were commercially available and used without further purification. Hexa(ethylene glycol) ditosylate (42), $Pt(PEt_3)_4$ (47), **5** (48), **9** (49), **10** (31), and **11** (50) were prepared according to the literature procedures. NMR spectra were recorded on a Varian Unity 300- or 400-MHz spectrometer. ^1H and ^{13}C NMR chemical shifts are reported relative to residual solvent signals, and $^{31}P\{^1H\}$ NMR chemical shifts are referenced to an external unlocked sample of 85% H_3PO_4 (δ 0.0 ppm). Mass spectra were recorded on a Micromass Quattro II triple-quadrupole mass spectrometer using electrospray ionization with a MassLynx operating system. The melting points were collected on an SHPSIC WRS-2 automatic melting point apparatus. The UV-vis experiments were conducted on a Hitachi U-4100 absorption spectrophotometer. The fluorescent experiments were conducted on a Hitachi F-7000 fluorescence spectrophotometer. Quantum yields were determined using quinine sulfate at 365 nm as reference (Φ_F = 56%).

Metallacycles **1**, **2**, and **3** were synthesized by stirring **8** with **10**, **11**, **or 12** in a 1:1 molar ratio at room temperature for 12 h. Then diethyl ether was added to the homogeneous solution to give the corresponding metallacycles as

precipitates. Bis-ammonium salt **4** was synthesized by the reaction of compound **14** with *n*-butylamine, followed by reduction, protonation, and ion exchange. The supramolecular assemblies were prepared by mixing metallacycles (**1**, **2**, or **3**) with **4** in a 1:1 molar ratio in acetone at room temperature.

Metallacycle **1**: ^{1}H NMR (400 MHz, CD_3COCD_3, 295 K): 9.11 (dd, J_1 = 12.1 Hz, J_2 = 5.4 Hz, 8H), 8.70 (s, 4H), 8.18 (d, J = 5.6 Hz, 8H), 8.01–8.23 (m, 18H), 7.82 (d, J = 8.5 Hz, 4H), 7.49 (d, J = 7.8 Hz, 8H), 7.29 (d, J = 7.8 Hz, 4H), 4.37–4.48 (m, 8H), 3.97–4.07 (m, 8H), 3.74–3.83 (m, 8H), 3.69–3.74 (m, 8H), 3.56–3.68 (m, 16H), 1.41–1.66 (m, 48H), 1.15–1.34 (m, 72H). ^{31}P{^{1}H} NMR (121.4 MHz, CD_3COCD_3, 295 K): 14.17 ppm (s, ^{195}Pt satellites, $^1J_{Pt–P}$ = 2,674.2 Hz). ESI-TOF-MS: *m/z* 896.3092 [**1** – 4OTf]$^{4+}$, 1244.7423 [**1** – 3OTf]$^{3+}$, 1,941.5898 [**1** – 2OTf]$^{2+}$.

Metallacycle **2**: ^{1}H NMR (400 MHz, CD_3COCD_3, 295 K): 9.06 (t, J = 6.2 Hz, 8H), 8.68 (s, 4H), 8.15 (dd, J_1 = 16.7 Hz, J_2 = 5.3 Hz, 8H), 8.04 (d, J = 8.4 Hz, 4H), 7.86 (d, J = 8.2 Hz, 8H), 7.82 (d, J = 8.6 Hz, 4H), 7.33 (d, J = 8.2 Hz, 8H), 7.10–7.29 (m, 20H), 4.37–4.52 (m, 8H), 3.98–4.08 (m, 8H), 3.75–3.82 (m, 8H), 3.68–3.75 (m, 8H), 3.61–3.68 (m, 16H), 1.41–1.62 (m, 48H), 1.14–1.30 (m, 72H). ^{31}P{^{1}H} NMR (121.4 MHz, CD_3COCD_3, 295 K): 14.69 ppm (s, ^{195}Pt satellites, $^1J_{Pt–P}$ = 2,784.6 Hz). ESI-TOF-MS: *m/z* 901.3514 [**2** – 4OTf]$^{4+}$, 1,252.1193 [**2** – 3OTf]$^{3+}$, 1,952.6388 [**2** – 2OTf]$^{2+}$.

Metallacycle **3**: ^{1}H NMR (400 MHz, CD_3COCD_3, 295 K): 9.09–9.30 (m, 8H), 8.69 (s, 4H), 8.21–8.47 (m, 12H), 7.94–8.18 (m, 24H), 7.79 (d, J = 7.0 Hz, 4H), 4.35–4.50 (m, 8H), 3.97–4.07 (m, 8H), 3.74–3.82 (m, 8H), 3.67–3.74 (m, 8H), 3.57–3.67 (m, 16H), 1.36–1.61 (m, 48H), 1.07–1.31 (m, 72H). ^{31}P{^{1}H} NMR (121.4 MHz, CD_3COCD_3, 295 K): 13.89 ppm (s, ^{195}Pt satellites, $^1J_{Pt–P}$ = 2655.5 Hz). ESI-TOF-MS: *m/z* 898.3780 [**3** – 4OTf]$^{4+}$, 1,247.4213 [**3** – 3OTf]$^{3+}$, 1,945.6079 [**3** – 2OTf]$^{2+}$.

ACKNOWLEDGMENTS. P.J.S. thanks National Science Foundation (Grant 1212799) for financial support. Y.S. thanks National Natural Science Foundation of China (Grants 21574034 and 21274034) and Zhejiang Provincial Natural Science Foundation of China (Grant LY16B040006) for financial support.

1. Dsouza RN, Pischel U, Nau WM (2011) Fluorescent dyes and their supramolecular host/guest complexes with macrocycles in aqueous solution. *Chem Rev* 111(12):7941–7980.
2. Lee MH, Kim JS, Sessler JL (2015) Small molecule-based ratiometric fluorescence probes for cations, anions, and biomolecules. *Chem Soc Rev* 44(13):4185–4191.
3. Daly B, Ling J, de Silva AP (2015) Current developments in fluorescent PET (photoinduced electron transfer) sensors and switches. *Chem Soc Rev* 44(13):4203–4211.
4. You L, Zha D, Anslyn EV (2015) Recent advances in supramolecular analytical chemistry using optical sensing. *Chem Rev* 115(15):7840–7892.
5. Li J, Yim D, Jang WD, Yoon J (2016) Recent progress in the design and applications of fluorescence probes containing crown ethers. *Chem Soc Rev*, 10.1039/C6CS00619A.
6. Schultz-Sikma EA, Meade TJ (2012) Supramolecular chemistry in biological imaging in vivo. *Supramolecular Chemistry: From Molecules to Nanomaterials*, eds Gale PA, Steed JW (John Wiley & Sons, Chichester, UK), pp 1851–1876.
7. Peng H-Q, et al. (2015) Biological applications of supramolecular assemblies designed for excitation energy transfer. *Chem Rev* 115(15):7502–7542.
8. Ma X, Zhao Y (2015) Biomedical applications of supramolecular systems based on host-guest interactions. *Chem Rev* 115(15):7794–7839.
9. Webber MJ, Appel EA, Meijer EW, Langer R (2016) Supramolecular biomaterials. *Nat Mater* 15(1):13–26.
10. Shi B, et al. (2016) Nanoparticles with near-infrared emission enhanced by pillararene-based molecular recognition in water. *J Am Chem Soc* 138(1):80–83.
11. Ajayaghosh A, Praveen VK, Vijayakumar C, George SJ (2007) Molecular wire encapsulated into pi organogels: Efficient supramolecular light-harvesting antennae with color-tunable emission. *Angew Chem Int Ed Engl* 46(33):6260–6265.
12. Abbel R, et al. (2009) White-light emitting hydrogen-bonded supramolecular copolymers based on pi-conjugated oligomers. *J Am Chem Soc* 131(2):833–843.
13. Chen P, Li Q, Grindy S, Holten-Andersen N (2015) White-light-emitting lanthanide metallogels with tunable luminescence and reversible stimuli-responsive properties. *J Am Chem Soc* 137(36):11590–11593.
14. Ni XL, Chen S, Yang Y, Tao Z (2016) Facile cucurbit[8]uril-based supramolecular approach to fabricate tunable luminescent materials in aqueous solution. *J Am Chem Soc* 138(19):6177–6183.
15. Zhang QW, et al. (2016) Multicolor photoluminescence including white-light emission by a single host-guest complex. *J Am Chem Soc* 138(41):13541–13550.
16. Stang PJ, Olenyuk B (1997) Self-assembly, symmetry, and molecular architecture: Coordination as the motif in the rational design of supramolecular metallacyclic polygons and polyhedra. *Acc Chem Res* 30(12):502–518.
17. Leininger S, Olenyuk B, Stang PJ (2000) Self-assembly of discrete cyclic nanostructures mediated by transition metals. *Chem Rev* 100(3):853–908.
18. Fujita M, Tominaga M, Hori A, Therrien B (2005) Coordination assemblies from a Pd(II)-cornered square complex. *Acc Chem Res* 38(4):369–378.
19. Oliveri CG, Ulmann PA, Wiester MJ, Mirkin CA (2008) Heteroligated supramolecular coordination complexes formed via the halide-induced ligand rearrangement reaction. *Acc Chem Res* 41(12):1618–1629.
20. Northrop BH, Zheng Y-R, Chi K-W, Stang PJ (2009) Self-organization in coordination-driven self-assembly. *Acc Chem Res* 42(10):1554–1563.
21. De S, Mahata K, Schmittel M (2010) Metal-coordination-driven dynamic heteroleptic architectures. *Chem Soc Rev* 39(5):1555–1575.
22. Chakrabarty R, Mukherjee PS, Stang PJ (2011) Supramolecular coordination: Self-assembly of finite two- and three-dimensional ensembles. *Chem Rev* 111(11):6810–6918.
23. Cook TR, Zheng Y-R, Stang PJ (2013) Metal-organic frameworks and self-assembled supramolecular coordination complexes: Comparing and contrasting the design, synthesis, and functionality of metal-organic materials. *Chem Rev* 113(1):734–777.
24. Brown CJ, Toste FD, Bergman RG, Raymond KN (2015) Supramolecular catalysis in metal-ligand cluster hosts. *Chem Rev* 115(9):3012–3035.
25. Cook TR, Stang PJ (2015) Recent developments in the preparation and chemistry of metallacycles and metallacages via coordination. *Chem Rev* 115(15):7001–7045.
26. Newkome GR, Moorefield CN (2015) From 1 → 3 dendritic designs to fractal supramacromolecular constructs: Understanding the pathway to the Sierpiński gasket. *Chem Soc Rev* 44(12):3954–3967.
27. McConnell AJ, Wood CS, Neelakandan PP, Nitschke JR (2015) Stimuli-responsive metal-ligand assemblies. *Chem Rev* 115(15):7729–7793.
28. Lifschitz AM, Rosen MS, McGuirk CM, Mirkin CA (2015) Allosteric supramolecular coordination constructs. *J Am Chem Soc* 137(23):7252–7261.
29. Saha ML, Yan X, Stang PJ (2016) Photophysical properties of organoplatinum(II) compounds and derived self-assembled metallacycles and metallacages: Fluorescence and its applications. *Acc Chem Res* 49(11):2527–2539.
30. Yan X, Cook TR, Wang P, Huang F, Stang PJ (2015) Highly emissive platinum(II) metallacages. *Nat Chem* 7(4):342–348.
31. Yan X, et al. (2015) A suite of tetraphenylethylene-based discrete organoplatinum(II) metallacycles: Controllable structure and stoichiometry, aggregation-induced emission, and nitroaromatics sensing. *J Am Chem Soc* 137(48):15276–15286.
32. Yan X, et al. (2016) Light-emitting superstructures with anion effect: Coordination-driven self-assembly of pure tetraphenylethylene metallacycles and metallacages. *J Am Chem Soc* 138(13):4580–4588.
33. Zhou Z, et al. (2016) Immobilizing tetraphenylethylene into fused metallacycles: Shape effects on fluorescence smission. *J Am Chem Soc* 138(40):13131–13134.
34. Zhang M, et al. (2016) Fluorescent metallacycle-cored polymers via covalent linkage and their use as contrast agents for cell imaging. *Proc Natl Acad Sci USA* 113(40):11100–11105.
35. Li Z, Kishi N, Hasegawa K, Akita M, Yoshizawa M (2011) Highly fluorescent M_2L_4 molecular capsules with anthracene shells. *Chem Commun (Camb)* 47(30):8605–8607.
36. Hong Y, Lam JWY, Tang BZ (2011) Aggregation-induced emission. *Chem Soc Rev* 40(11):5361–5388.
37. Zhao Z, Lam JWY, Tang BZ (2012) Tetraphenylethene: A versatile AIE building block for the construction of efficient luminescent materials for organic light-emitting diodes. *J Mater Chem* 22(45):23726–23740.
38. Mei J, et al. (2014) Aggregation-induced emission: The whole is more brilliant than the parts. *Adv Mater* 26(31):5429–5479.
39. Mei J, Leung NL, Kwok RT, Lam JW, Tang BZ (2015) Aggregation-induced emission: Together we shine, united we soar! *Chem Rev* 115(21):11718–11940.
40. Yamashina M, et al. (2015) Preparation of highly fluorescent host–guest complexes with tunable color upon encapsulation. *J Am Chem Soc* 137(29):9266–9269.
41. Zhou Z, Yan X, Cook TR, Saha ML, Stang PJ (2016) Engineering functionalization in a supramolecular polymer: Hierarchical self-organization of triply orthogonal non-covalent interactions on a supramolecular coordination complex platform. *J Am Chem Soc* 138(3):806–809.
42. Zhang C, et al. (2007) Benzo-21-crown-7/secondary dialkylammonium salt [2]pseudorotaxane- and [2]rotaxane-type threaded structures. *Org Lett* 9(26):5553–5556.
43. De Greef TFA, et al. (2009) Supramolecular polymerization. *Chem Rev* 109(11):5687–5754.
44. Yang L, Tan X, Wang Z, Zhang X (2015) Supramolecular polymers: Historical development, preparation, characterization, and functions. *Chem Rev* 115(15):7196–7239.
45. Yan X, et al. (2013) Supramolecular polymers with tunable topologies via hierarchical coordination-driven self-assembly and hydrogen bonding interfaces. *Proc Natl Acad Sci USA* 110(39):15585–15590.
46. Liu Y, Wang Z, Zhang X (2012) Characterization of supramolecular polymers. *Chem Soc Rev* 41(18):5922–5932.
47. Yoshida T, Matsuda T, Otsuka S, Parshall GW, Peet WG (1990) Tetrakis(triethylphosphine)platinum(0). *Inorg Synth* 28:122–123.
48. Kim HJ, Lee E, Park HS, Lee M (2007) Dynamic extension-contraction motion in supramolecular springs. *J Am Chem Soc* 129(36):10994–10995.
49. Ashton PR, et al. (1996) Pseudorotaxanes formed between secondary dialkylammonium salts and crown ethers. *Chemistry* 2(6):709–728.
50. Qu Y, et al. (2013) A new triphenylamine fluorescent dye for sensing of cyanide anion in living cell. *Tetrahedron Lett* 54(36):4942–4944.